

# Microfabricated arrays of femtoliter chambers allow single molecule enzymology

Yannick Rondelez<sup>1</sup>, Guillaume Tresset<sup>1</sup>, Kazuhito V Tabata<sup>2,3</sup>, Hideyuki Arata<sup>2</sup>, Hiroyuki Fujita<sup>2</sup>, Shoji Takeuchi<sup>2</sup> & Hiroyuki Noji<sup>2</sup>

Precise understanding of biological functions requires tools comparable in size to the basic components of life<sup>1–4</sup>. Single molecule studies have revealed molecular behaviors usually hidden in the ensemble- and time-averaging of bulk experiments<sup>5,6</sup>. Although most such approaches rely on sophisticated optical strategies to limit the detection volume<sup>7,8</sup>, another attractive approach is to perform the assay inside very small containers<sup>9–16</sup>. We have developed a silicone device presenting a large array of micrometer-sized cavities. We used it to tightly enclose volumes of solution, as low as femtoliters, over long periods of time. The microchip insures that the chambers are uniform and precisely positioned. We demonstrated the feasibility of our approach by measuring the activity of single molecules of  $\beta$ -galactosidase and horseradish peroxidase. The approach should be of interest for many ultrasensitive bioassays at the single-molecule level.

Liposomes<sup>12,14</sup>, oil-dispersed droplets<sup>11,16</sup>, chip-based<sup>10,13</sup> and other strategies<sup>15,17</sup> have been used to confine ultrasmall water samples. As the working volume is reduced, it becomes difficult to control evaporation, which becomes severe at the nanoliter level<sup>15,16</sup>; the dimensions and monodispersity of the reactor volume<sup>17</sup>; and well-defined, preset positioning of the droplets to facilitate observation<sup>12,18</sup>. Micro/nanotechnologies allow the design of very small arrayed structures (1 fl = 1  $\mu\text{m}^3$ ) and are well-suited to address these challenges, while simultaneously allowing large-scale integration<sup>4</sup>.

In combination with microscopic techniques such as total internal reflection fluorescence or confocal microscopy, microfabricated chips have been applied to single-molecule detection<sup>8,10</sup>, allowing fine confinement of the observation volume. However, their use to inhibit the diffusion of the reaction products at the single enzyme level has not yet been demonstrated.

To build the device, we selected poly-dimethylsiloxane (PDMS), a silicone elastomer that is transparent to visible light and spontaneously adhesive to smooth surfaces. The PDMS matrix has a low affinity for hydrophilic molecules and its surface can be passivated against biomolecules<sup>19</sup>. This material is easily patterned through molding techniques<sup>20</sup>. We prepared a silicon wafer displaying arrays of regular cylindrical features at the micrometer scale (Fig. 1) and used it as a master template to produce series of identical PDMS sheets by molding. Scanning electron microscopy (SEM) showed regularly spaced, uniformly shaped cylindrical chamber. To introduce the buffer solution inside the cavities, we sandwiched a droplet between a microscope slide and the patterned PDMS sheet, achieving a homogeneous distribution by capillarity. Under pressure, gas bubbles and excess water were evacuated, and Van der Waals forces<sup>20</sup> were

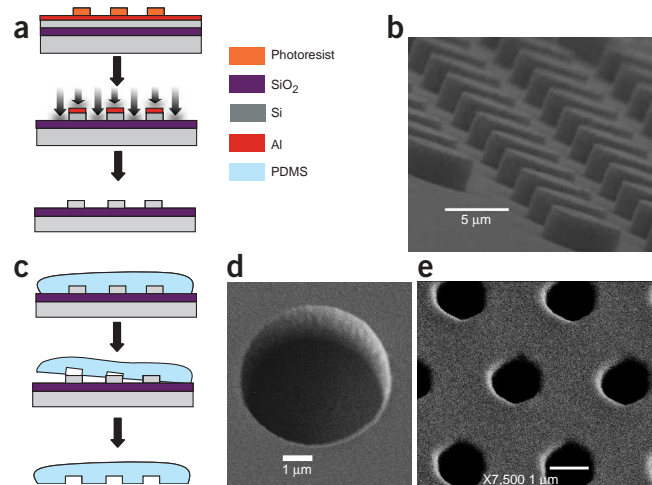


**Figure 1** Microfabrication of the PDMS chambers. (a) Fabrication of the mold: a 1.5- $\mu\text{m}$ -thick SOI wafer was covered with an aluminum mask, itself patterned by photolithography. After etching and removing the aluminum layer, the silicon surface showed regular arrays of identical cylindrical shapes. (b) SEM image of the silicon mold, in a region patterned with 5- $\mu\text{m}$  microstructures. This technique allows a precise control of the shapes of the chambers. (c) After Teflon coating of the mold, liquid PDMS was poured, cured at 90  $^{\circ}\text{C}$  for polymerization and peeled off. (d,e) SEM images of the PDMS sheets: mold patterns were precisely reproduced at both the 5- $\mu\text{m}$  (d) and the 1- $\mu\text{m}$  (e) level, for which the chambers had an internal volume of 1.4 fl.

<sup>1</sup>Laboratory for Integrated Micro Mechatronic Systems (LIMMS-CNRS/IIS), <sup>2</sup>Institute of Industrial Science (IIS), University of Tokyo, 4-6-1 Komaba, Meguroku, 153-8505 Tokyo, Japan. <sup>3</sup>Research on Advanced Medical Technology, Japan Association for the Advancement of Medical Equipment (JAAME), 3-42-6, Hongo, Bunkyo-ku, Tokyo, Japan. Correspondence should be addressed to H.N. (hnoji@iis.u-tokyo.ac.jp).

sufficient to bond the PDMS to the glass surface. As demonstrated below, this step distributes the buffer among up to  $10^5$  independent reaction vessels per  $\text{mm}^2$ , each of them containing a few femtoliters of liquid solution (Fig. 2).

The resultant femtoliter chambers were inspected for possible leaks or evaporation. To do so, fluorescent beads (200 nm) or quantum dots ( $6 \times 12$  nm) were enclosed in the variously sized chambers (1.4–100 fl). Their brownian motion was observed over more than 1 h (Supplementary Video online), proving the presence of a stable liquid phase. Moreover, no escapes from the chambers were ever recorded and the possibility of connecting water channels was then eliminated.

PDMS is known to have an affinity for hydrophobic molecules. As a result, some lipophilic compounds (that is, having a high octanol/water partition coefficient) can be transported through PDMS membranes<sup>21,22</sup>. We checked that hydrophilic solutes could not diffuse through the walls of the chambers. The whole array was filled with various negatively charged fluorescent dye solutions and sealed. Then, using a pinhole, one of the chambers was photobleached for a few seconds. Subsequent recording of the intensity proved that the dye could not diffuse from the unaffected chambers to the bleached one, which remained dark over the 20 min of the test<sup>23</sup> (Fig. 2e). In a reverse experiment, we switched on the fluorescence of a few chambers, by using a caged fluorescent compound and selective UV illumination. Again, no diffusion was observed (Fig. 2g). It thus appears that PDMS acted as an impermeable barrier for water-soluble compounds, and tightly enclosed each chamber. These experiments also show that, whereas all the chambers contain the same starting solution, they remain addressable individually by simple means, such as light in the present case.

When the volume decreases, surface-to-volume ratios, and hence surface effects, increase drastically, presumably leading to surface denaturation of the biomolecules present in the sample<sup>24</sup>. In the case of PDMS, this effect can be minimized by coating the surface with an excess amount of BSA<sup>25</sup>. To check that these chambers were suitable for biological studies, we used a starting solution containing DNA fragments and an intercalating fluorescent dye. As with beads, the brownian motion of the DNA fragment could be observed in the chambers, without apparent surface binding or diffusion to a neighboring chamber (Fig. 2d). Under these conditions, the usual solution dynamic of the DNA chains was preserved, which opens the use of this device for single DNA chips<sup>13,16</sup>.

In the case of enzymes, the microarray allows both the proteins and their substrate/products to be trapped in the same chamber. Because of the extremely small volume, a minute quantity of enzymatic products is enough to reach a detectable concentration, and we can therefore expect to detect directly the individual activities of isolated single enzymes. We have demonstrated this idea using  $\beta$ -galactosidase ( $\beta$ -Gal) or horseradish peroxidase (HRP) as model enzymes. A fluorogenic commercial activity assay mixture (Supplementary Fig. 2 online) was distributed over the whole array<sup>26</sup> of 30-fl

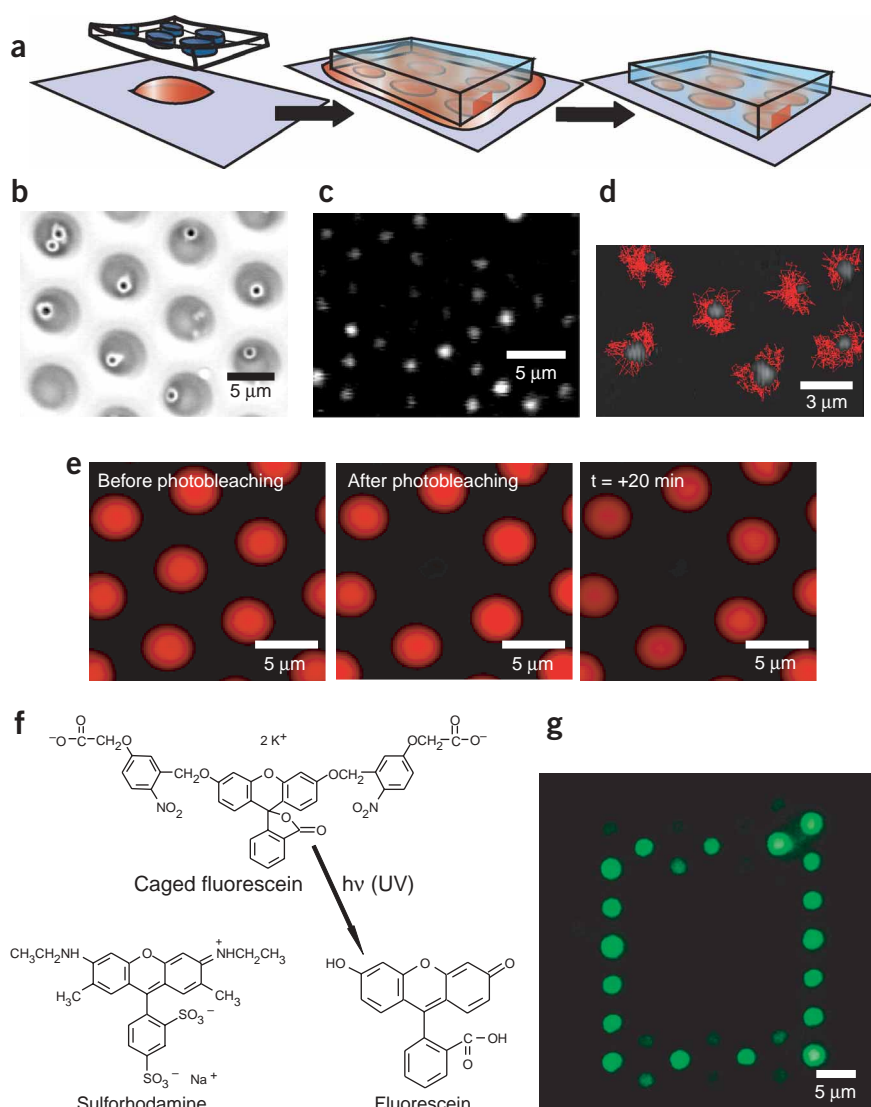


**Figure 2** Water enclosure in the microchambers, and evaluation of the sealing. **(a)** Sealing process: the buffer solution that contains the molecules of interest is sandwiched between a glass plate and the PDMS layer. Upon pressure, PDMS attached tightly to the glass surface and closed the chambers, impeding diffusion. **(b–d)** Inclusion of plastic beads **(b)**, quantum dots **(c)** and  $\lambda$ -DNA chains **(d)** in variously sized microchambers. The images have been superimposed with the recording of the 2-min trajectory of single DNA molecules undergoing brownian motion in the chambers. No jumps to a neighboring chamber were observed. **(e)** Photobleaching experiment using sulforhodamineG (see **f**). Upper and middle images show the central chamber just before and just after photobleaching, respectively; lower one was taken 20 min later. Diffusion of the dye across the PDMS, which would result in an increase of the fluorescent intensity in the central chamber, was not observed. Structures of fluorescence dyes used in the photobleaching and photoreleasing experiments. **(g)** A caged fluorescein compound (see **f**) can be activated selectively inside a few chambers using a focused UV-light beam. Here, a square shape was first drawn before recording the fluorescent intensity under visible light.

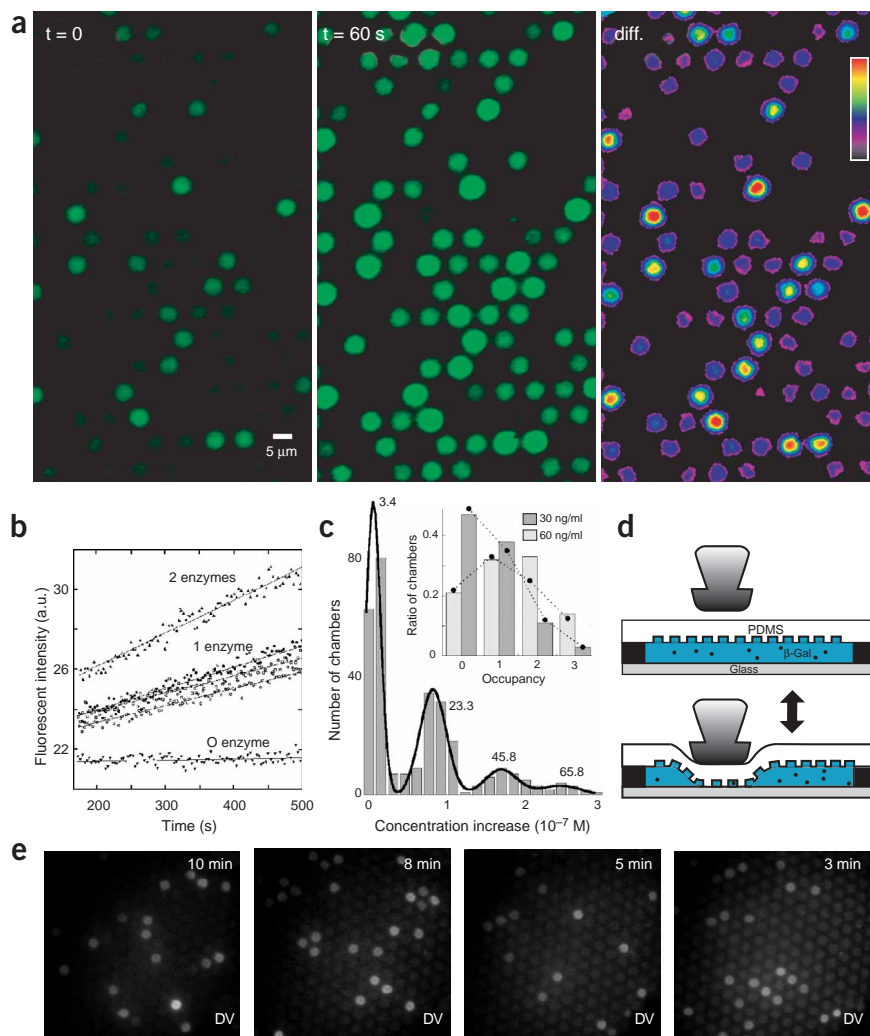
containers. After closing, we measured the fluorescent intensity simultaneously in  $\sim 300$  chambers, using a microscope. When the enzyme solution was diluted down to a ratio close to 1:1 enzyme per chamber, it appeared that the brightness in the array was not homogeneously distributed (Fig. 3a). More precisely, the intensity was quantized among a few discrete levels: dark, medium and bright chambers were easily distinguished. Real-time recording of the enzymatic activity in each chamber also revealed a quantization in the rate of fluorescent increase (Fig. 3b). The histogram of the fluorescence increment in 60 s showed four well-defined peaks, that we could attribute to the presence of zero, one, two or three enzymes, respectively, in the corresponding chamber. The peaks were regularly spaced, and the turnover rate of a single enzyme could be derived from the increment value (Fig. 3c for  $\beta$ -Gal and Supplementary Fig. 1 online for HRP). In the case of  $\beta$ -Gal, we determined it to be  $20 \text{ s}^{-1}$ , which is consistent with an earlier report<sup>26</sup> of  $17 \text{ s}^{-1}$ . The area under each peak corresponds to the number of chambers containing zero, one, two or three enzymes. The resulting histogram was consistent with poisson statistics, as expected for a random distribution of molecules inside

the chambers. The fitting parameter yielded the ratio of enzyme per chamber, which in turn gave the true active enzyme concentration. We observed that more than 70% of the introduced enzyme had remained active. If the chambers were then opened and closed again, activity was observed at a different, random position (Fig. 3d,e). This shows that enzymes are not surface bound, but are indeed free in solution throughout the assay. Thus, this device detected catalytic outcomes of single enzymes without interfering with their activity.

We have demonstrated the formation of femtoliter water volumes, obtained by enclosing a liquid solution between a micropatterned silicone sheet and a microscope glass slide. From the microscopic observation of entrapped plastic beads, quantum dots or fluorescent dyes, we have carefully evaluated the stability of the water droplets. It was shown that PDMS is sufficiently impermeable to inhibit evaporation or leakage over a typical bioassay time. For the isolation of stable, regular and arrayed volumes of water, this technique represents an improvement of several orders of magnitude compared with previous results<sup>13</sup>.

**Figure 3** Detection of the activity of single  $\beta$ -galactosidase molecules. (a) Fluorescent images of the enzymatic activity in the chambers:  $\beta$ -Gal hydrolyzes fluorescein-di- $\beta$ -D-galactopyranoside to fluorescein (see Supplementary Fig. 2 online). A low concentration of the enzyme was dispersed and enclosed in an array of 30-fL chambers. Fluorescent images were recorded just after closing the chambers (left panel), and 1 min later (middle panel). The right panel, diff., shows the intensity difference between these two images, in the form of a color gradient.

The intensities, which are proportional to the enzymatic activity in each chamber, show a clear quantization. (b) Continuous recording of  $\beta$ -Gal activity. Using low light intensity, the fluorescent increase in the same chambers is measured in a continuous manner. After averaging the intensity over 1 s, five representative chambers have been plotted. Whereas ( $\blacktriangledown$ ) appears to contain no enzyme, ( $\bullet$ ), ( $\square$ ) and ( $\circ$ ) have one  $\beta$ -Gal and ( $\blacktriangle$ ) two. Over this time period, activity is observed as a continuous increase in the product concentration, showing that the enzymes are not temporarily inactivated as a result of surface interactions. (c) In the histogram the number of chambers is plotted versus the increase in concentration over 60 s (experiment in a). The four peaks can be attributed to an occupancy of 0, 1, 2 or 3 enzymes per chamber. They were fitted with a sum of gaussians. The values displayed next to each peak are the centers of these gaussians, converted to specific activity ( $\text{s}^{-1}$ ). The insert shows the occupancy distribution for the experiment in a ( $\beta$ -Gal 30 ng/ml, in gray), together with another experiment using a two-fold concentration of the enzyme (60 ng/ml, light gray). The bars show the ratio ( $x$ ) of chambers with an occupancy of  $N$  enzymes ( $N = 0, 1, 2, 3$ ). Spots are the fitting to the statistical poisson distribution  $x = \mu^N \cdot e^{-\mu} / N!$ , where the parameter  $\mu$  yields the average number of enzymes per chamber. The good fit and quantitatively consistent  $\mu$  values (0.72 in gray and 1.51 in light gray, corresponding to 71% and 75% of the introduced protein concentration) confirm the previous attribution. (d) By pressing a small area of the PDMS sheet with a glass needle, successive opening/closing rounds could be performed, allowing the exchange of the content of each chamber. (e) Four successive rounds, showing that after each closing,  $\beta$ -Gal activity appeared at random positions, thus ruling out nonspecific surface binding of the enzyme.



Such extremely small volumes push forward the limits of fluorescent detection to impressively low values. With this simple setup, we found a detection limit of 10 molecules only in the smallest chambers of 1.4 fl (corresponding to 10 nM of fluorescein). We have used these advantages to perform an enzymatic assay at the single-molecule level. Indeed, when they are trapped in a femtoliter chamber, single  $\beta$ -Gal and HRP molecules need only a few turnovers to accumulate a detectable concentration of their fluorescent products. Most single-molecule techniques are blind to the enzymatic reaction product; they monitor conformational changes of the enzyme itself<sup>5,27</sup>, or its binding/releasing events, but without discriminating catalytic product from substrate<sup>7,28</sup>. By contrast, we have directly detected catalytic product. Such information is essential when studying, for example, the coupling efficiency of enzymatic processes<sup>29</sup>. Furthermore, the precise positioning of homogeneous chambers gave us easy access to statistical analysis. Thereby, we have independently obtained both the turnover rate and the concentration of enzymes that are active. Such values are difficult to access otherwise.

Ultrasmall volumes are desirable for biotechnology applications because of their low product requirement, fast detection and high parallelism<sup>1,3</sup>. Here, we have shown that such microcontainers allow the quantitative detection of a single enzyme's reaction products. We have recently succeeded in measuring the coupling efficiency of a molecular motor by monitoring real chemical output at the single-molecule level using this technique<sup>30</sup>. We also expect applications in the field of ultrasensitive detection, where the microchamber approach does not require the usual surface-binding strategies, and offers the possibility of working directly in solution. This allows the study of multiple proteins or even single living cells. Microchamber arrays might also offer the possibility to study full populations of similar enzymes displaying nonhomogeneous activity<sup>5,6</sup>, due, for example, to post-transcriptional modifications.

## METHODS

**Microfabrication.** Arrays of small cylinders, including variations in the diameter (from 1–8  $\mu\text{m}$ ) and the step size (from 1–10  $\mu\text{m}$ ) were fabricated from a 1.5  $\mu\text{m}$  thick Silicon on Insulator (SOI) wafer (Soitec) by Inductive Coupled Plasma–Reactive Ion Etching. An aluminum layer was evaporated onto the SOI to serve as a mask for plasma etching and patterned by using 0.5- $\mu\text{m}$  thick photoresist (S1805, Shipley) exposed with a mask aligner (Union). Photoresist and aluminum were washed away after the deep-RIE process. PDMS sheets were obtained from this master, which had been treated with  $\text{CHF}_3$  plasma (100-nm thick) to facilitate the removal. Actual diameters of the chambers were measured using SEM (JSM-7400F, JEOL). Volume for the smallest chambers were  $1.40 \pm 0.08$  fl.

**Imaging.** Fluorescent recording were taken under an Olympus IX71 microscope equipped with an Hg lamp, the appropriate filter sets (Omega optical), and a CCD (300-RCX, MTI) working at 30 frames per second, coupled with a light intensifier (VS4-1845, Videoscope). To decrease background, a diaphragm was used, and a pinhole in the focal plane of the light line allowed the illumination of a reduced zone of the PDMS sheet. The intensity was recorded through a 60 $\times$  or 100 $\times$  objective lens (Olympus, NA 1.25–1.30). Analysis was done with a custom-made software. Colors were added afterwards.

**Chemicals.** The experiments were conducted in a 100 mM phosphate buffer pH = 7.5, in the presence of 0.05 to 10 mg/ml BSA, 1 mM  $\text{MgCl}_2$  and 2  $\mu\text{l/ml}$  mercaptoethanol. Fluorescein di- $\beta$ -D-galactopyranoside (FDG), fluorescein, Bodipy492/515disulfonate, sulforhodamineG,

SYBRGreen and fluorescent beads were from Molecular Probes and quantum dots from Quantum Dot Corp.  $\beta$ -galactosidase (Roche) was expressed in *E. coli*. Sealing was obtained by simply pressing vertically the PDMS against the glass plate. The PDMS sheet was topped with a second glass plate to prevent evaporation. After the experiment, the PDMS sheet could be washed and used again.

**Photobleaching experiment.** Fluorescence bleaching experiments were conducted with Bodipy492/515, sulforhodamineG and fluorescein at concentrations of 1–2  $\mu\text{M}$ , yielding positive results as those shown in **Figure 2**. To allow for longer time recording, the chambers were illuminated only stepwise, 2 s every min. Fluorescent records displayed in the figures are averaged over 0.15 s (five frames).

**Biological assays in chambers.** For the DNA experiments,  $\lambda$ -DNA strands (4 ng/ $\mu\text{l}$ ) were stained with SyberGreen at a 1/10,000 dilution. Chambers were closed as usual and observed under a fluorescent microscope.  $\beta$ -galactosidase activity measurements were performed at a high (200  $\mu\text{M}$ ) concentration of FDG, to ensure a one-step catalysis<sup>26</sup>. Chambers were kept in the dark during the experiment, and fluorescence intensity was recorded at 1 min intervals. The intensity in 300 randomly selected chambers (present on one screen) was used for the histogram. Rates were calculated by comparison with fluorescein standards. Using the same conditions, except for the presence of a larger amount of mercaptoethanol, Huang found the  $k_{\text{cat}}$  to be 17.1  $\text{s}^{-1}$ . In the various experiments, the concentration of  $\beta$ -Gal found in the chambers represented 80–90% of expected, calculated from the sample specifications.

**Opening/closing experiment.** For opening/closing experiments, we used thin spacers to suspend the PDMS layer over the glass slide, thereby enclosing a few microliters of the bulk buffer. In this situation, every chamber (6 fl) is opened to the bulk of the solution (see **Fig. 3**). Then using a small pusher, a small fraction of the chambers was closed by pressing them against the glass slide. We allowed 2 min for the reaction to take place, after which a fluorescent image was recorded. Releasing the pressure took the system back to the initial state and the sequence was repeated 3 times to obtain the sequential images in **Fig. 3**. Increase in the background intensity was caused by the catalytic reaction also taking place in the bulk of the buffer over the 10 min necessary to complete the experiment.

*Note: Supplementary information is available on the Nature Biotechnology website.*

## ACKNOWLEDGMENTS

This project was performed in the framework of the Laboratory for Integrated Micro Mechatronic Systems (LIMMS-CNRS/IIS), and financially supported by the Japan Society for the Promotion of Science (H.N., S.T. and H.F.), Bio-Oriented Technology Research Advancement Institution (H.N. and S.T.) and Mitsubishi Foundation (H.N. and S.T.). We thank all members of Noji, Takeuchi and Fujita laboratories for help and advice, and I. Baba and T. Kitamori for critical reading and R. Yasuda for programming of image analysis software. Y.R. and G.T. are Research Fellows of the Japan Society for the Promotion of Science.

## COMPETING INTERESTS STATEMENT

The authors declare that they have no competing financial interests.

Received 12 February; accepted 20 September 2004

Published online at <http://www.nature.com/naturebiotechnology/>

- Whitesides, G.M. The “right” size in nanobiotechnology. *Nat. Biotechnol.* **21**, 1161–1165 (2003).
- Jensen, K. Smaller, faster chemistry. *Nature* **393**, 735–736 (1998).
- Wölcke, J. & Ullmann, D. Miniaturized HTS technologies – uHTS. *Drug Discov. Today* **6**, 637–646 (2001).

4. Thorsen, T., Maerkl, S.J. & Quake, S.R. Microfluidic large scale interaction. *Science* **298**, 580–584 (2002).
5. Lu, H.P., Xun, L. & Xie, S. Single molecule enzymatic dynamics. *Science* **282**, 1877–1882 (1998).
6. Xue, Q. & Yeung, E. Differences in the chemical reactivity of individual molecules of an enzyme. *Nature* **373**, 681–683 (1995).
7. Funatsu, T. *et al.* Imaging of single molecules and individual ATP turnovers by single myosin molecules in aqueous solution. *Nature* **374**, 555–559 (1995).
8. Levene, M.J. *et al.* Zero-mode waveguides for single-molecule analysis at high concentrations. *Science* **299**, 682–686 (2003).
9. Lipman, A.E., Shuler, B., Bakajin, O. & Eaton, W.A. Single molecule measurement of protein folding kinetics. *Science* **301**, 1233–1235 (2003).
10. Foquet, M., Korch, J., Zipfel, W.R., Webb, W.W. & Craighead, H.G. Focal volume confinement by submicrometer-sized fluidic channels. *Anal. Chem.* **76**, 1618–1626 (2004).
11. Gratzl, M., Lu, H., Matsimoto, T., Yi, C. & Bright, G.R. Fine chemical manipulations of microscopic liquid samples. 1. Droplet loading with chemicals. *Anal. Chem.* **71**, 2751–2756 (1999).
12. Stamou, S., Duschl, C., Delamarche, E. & Vogel, H. Self assembled micro-arrays of attoliter molecular vessels. *Angew. Chem. Int. Ed.* **42**, 5580–5583 (2003).
13. Nagai, H., Murakami, Y., Yokoyama, K. & Tamiya, E. High-throughput PCR in silicon based microchamber array. *Biosens. Bioelectron.* **16**, 1015–1019 (2001).
14. Chiu, D.T. *et al.* Chemical transformations in individual ultrasmall biomimetic containers. *Science* **283**, 1892–1895 (1999).
15. Gosalia, D.N. & Diamond, S.L. Printing chemical library on microarrays for fluid phase nanoliter reactions. *Proc. Nat. Acad. Sci. USA* **100**, 8721–8726 (2003).
16. Nakano, M. *et al.* Single molecule PCR using water in oil emulsion. *J. Biotechnol.* **102**, 117–124 (2003).
17. Loscertales, I.G. *et al.* Micro/nano encapsulation via electrified coaxial liquid jets. *Science* **295**, 1695–1698 (2002).
18. Renault, J.P. *et al.* Fabricating arrays of single protein molecules on glass using microcontact printing. *J. Phys. Chem.* **107**, 703–711 (2003).
19. McDonald, J.C. & Whitesides, G.M. Poly(dimethylsiloxane) as a material for fabricating microfluidic devices. *Accounts Chem. Res.* **35**, 491–499 (2002).
20. Baltussen, E., Sandra, P., David, F., Janseen, H.G. & Cramers, C. Study of the equilibrium mechanism between water and PDMS for very apolar solutes: adsorption or sorption? *Anal. Chem.* **71**, 5213–5216 (1999).
21. Du Plessis, J., Pugh, J., Judefeind, A. & Hadgraft, J. The effect of the nature of H-bonding groups on diffusion through PDMS membranes saturated with octanol and toluene. *Eur. J. Pharm. Sci.* **15**, 62–69 (2002).
22. Rondelez, Y. *et al.* Femtoliters chambers for the study of mechanically-driven ATP synthesis by F1 protein motor. in *Proceedings of the 7th International Conference on Micro Total Analysis Systems*, 555–558, Squaw Valley, CA, USA, October 5–9, 2003.
23. Horbett, T.A. & Bratsh, J.L. Proteins at interfaces. in *Proteins at interfaces. Physico-chemical and biochemical studies* (eds. Brasch, J.L. & Horbett, T.A.) 1–33 (Amer. Chem. Soc., Washington, DC, 1987).
24. Wheeler, A.R. *et al.* Microfluidic device for single cell analysis. *Anal. Chem.* **75**, 3581–3586 (2003).
25. Sapsford, K.E. & Ligler, F.S. Realtime analysis of protein adsorption to a variety of thin films. *Biosensors and Bioelectronics* **19**, 1045–1055 (2004).
26. Huang, Z. Kinetic fluorescence measurement of fluorescein di- $\beta$ -galactoside hydrolysis by  $\beta$ -Galactosidase: intermediate channelling in stepwise catalysis by a free single enzyme. *Biochemistry* **30**, 8535–8540 (1991).
27. Noji, H., Yasuda, R., Yoshida, M. & Kinosita, K. Jr. Direct observation of the rotation of F<sub>1</sub>-ATPase. *Nature* **386**, 299–302 (1997).
28. Ishijima, A. & Yanagida, T. Single molecule nanobiotechnology. *Trends. Bio. Sci.* **26**, 438–444 (2001).
29. Itoh, H. *et al.* Mechanically driven ATP synthesis by F1-ATPase. *Nature* **427**, 465–468 (2004).
30. Rondelez, Y. *et al.* Highly coupled ATP synthesis by F1-ATPase single molecules. *Nature* **433**, 773–777 (2005).